

Frequency-dependent time lags in the X-ray emission of the Seyfert galaxy NGC 7469

I. E. Papadakis¹, K. Nandra^{2,3} and D. Kazanas⁴

ABSTRACT

We report the discovery of time lags in the cross-spectra of the X-ray light curves of the Seyfert galaxy NGC 7469. This behavior is common in Galactic black hole and neutron star binaries, and is in the sense that harder X-rays are delayed with respect to the soft with a time lag approximately proportional to the Fourier period. At the longest period probed by our observation (~ 6 days) we find a time lag of approximately 3.5 hours between the 2-4 and 4-10 keV X-rays. A similar lag and period dependence is found comparing the 2-4 and 10-15 keV light curves, albeit with less significance. We find the coherence function of the light curves to be close to 1 in the frequency range between $10^{-5.5} - 10^{-3.5}$ Hz. The implications of these results for the X-ray production mechanism in active galactic nuclei (AGN) is discussed.

Subject headings: galaxies: active – galaxies: nuclei – galaxies: individual (NGC 7469) – X-rays: galaxies

1. INTRODUCTION

Both stellar mass and supermassive black holes show persistent, rapid, large amplitude variations in their X-ray flux. Analysis of this variability can be a powerful diagnostic of the

¹Department of Physics, University of Crete, 71003, Heraklion, Greece

²Laboratory for High Energy Astrophysics, Code 662, NASA/Goddard Space Flight Center, Greenbelt, MD 20771

³Universities Space Research Association

⁴Laboratory for High Energy Astrophysics, Code 661, NASA/Goddard Space Flight Center, Greenbelt, MD 20771

emission processes in accreting compact objects. The variability is usually characterized by the power spectral density (PSD) function which has a steep “red noise” form that flattens below a characteristic break frequency. The dominant radiation mechanism in these objects is thought to be inverse Compton scattering of soft “seed” photons by a hot plasma (e.g. Shapiro, Lightman & Eardley 1976, Sunyaev & Titarchuk 1980). A general prediction of these models is that hard X-ray variations should lag those in softer bands, as former photons undergo more scatterings in the Comptonizing plasma.

Time lags have been observed in the Fourier cross-spectrum of both persistent and transient galactic black hole candidates (GBHC; e.g. Miyamoto et al. 1988, 1991). These observations lend strong support to the Comptonization hypothesis as they indeed show that the soft X-ray variations precede the hard. The observed time lag is an increasing function of Fourier period, i.e. the more slowly varying components show a longer time lag. In the most famous case, Cyg X-1, the lags increase from 10^{-4} s on a time scale of 0.01s, flattening out to 0.1 above a period of about 10s.

The variability properties of Galactic and extragalactic black holes are quite similar. For example, the form of the power spectra is very similar, with both classes showing evidence for a low-frequency “knee” (e.g. Edelson & Nandra 1999; McHardy et al. 1998) and a high frequency “break” (e.g. Nowak & Chiang 2000). One AGN with a particularly well-sampled X-ray light curve is NGC 7469 (Nandra et al. 1998). Nandra et al. (2000) have shown that the X-ray spectral shape correlates with the ultraviolet flux in this object. This is highly suggestive of the seed photons cooling the Comptonizing plasma (e.g. Pietrini & Krolik 1995; Petrucci et al. 2000). Nandra & Papadakis (2001; hereafter NP01) found further support for the Comptonization model in that the cross-correlation functions (CCF) between X-ray light curves in various bands were asymmetric towards positive lags (i.e. in the sense that the soft X-ray variations preceded those in the harder bands). The variability amplitude was found to be larger in the soft band also, at least on long time scales. Contrary to the Comptonization hypothesis, however, NP01 found evidence that the high frequency PSD “hardens” (i.e. flattens) as a function of energy. This behavior is also seen in Cyg X-1 (Nowak et al. 1999a), further extending the suite of similarities between AGN and GBHC.

Comparison between GBHCs and AGN has not been extended to the cross-spectra, mostly because datasets of sufficiently high quality and sampling have not been obtained for AGN. An exception is the NGC 7469 dataset just mentioned, and in this Letter we present an analysis of its cross spectrum.

2. ANALYSIS TECHNIQUES

2.1. Phase spectrum and coherence function

Let $x_s(t)$ and $x_h(t)$ be the X-ray flux light curves in two energy bands (s and h stand for “soft” and “hard”), and let $R_s(k)$ and $R_h(k)$ denote the auto-covariance function of the two processes at lag k ($R(k) = E\{[x(t) - \bar{x}][x(t+k) - \bar{x}]\}$, where E is the expectation operator). The power spectral density of the processes is then defined as $P(\omega) = (1/2\pi) \int R(k)e^{-ik\omega} dk$. The functions $R_s(k), R_h(k)$, in the time domain, and $P_s(\omega), P_h(\omega)$, in the frequency domain, characterize the variability properties of the individual time series. If the two series are related, the correlation structure between them is characterized by the cross-covariance function, $R_{sh}(k) = E\{[x_s(t) - \bar{x}_s][x_h(t+k) - \bar{x}_h]\}$ and, in the frequency domain, by its Fourier transform, the cross-power spectral density function (or simply cross-spectrum), $P_{sh}(\omega) = (1/2\pi) \int R_{sh}(k)e^{-ik\omega} dk$. While $P(\omega)d\omega$ represents the contribution to the time series variance of the components with frequency ω , $P_{sh}(\omega)$ represents the covariance between these components in the two processes.

Unlike the PSD, the cross-spectrum is a complex function, since $R_{sh}(k)$ need not be a symmetric function around $k = 0$. Therefore, it can be written as: $P_{sh}(\omega) = c_{sh}(\omega) + iq_{sh}(\omega) = |a_{sh}(\omega)|e^{i\phi_{sh}(\omega)}$. The cross-spectrum amplitude, $|a_{sh}(\omega)| = \sqrt{c_{sh}(\omega)^2 + q_{sh}(\omega)^2}$, represents the average value of the product of the amplitudes of the components with frequency ω in $x_s(t)$ and $x_h(t)$. The function $\phi_{sh}(\omega) = \tan^{-1}[q_{sh}(\omega)/c_{sh}(\omega)]$ is called the phase-spectrum and represents the average value of the phase shift, $\phi_h(\omega) - \phi_s(\omega)$, between the components at frequency ω in $x_s(t)$ and $x_h(t)$. The corresponding time shift is given by $\tau(\omega) = \phi_{sh}(\omega)/\omega$. Finally, the coherence function is defined as: $\gamma^2(\omega) = |P_{sh}(\omega)|^2/[P_s(\omega)^2P_h(\omega)^2]$ (Vaughan & Nowak 1997) and gives the fraction of the mean-squared variability of one time series at ω that can be attributed to the other (Nowak et al. 1999a).

2.2. Estimation of lags and coherence function.

Consider N observations of the processes $x_{s,h}(t)$ for $t = 1\Delta t, 2\Delta t, \dots, N\Delta t$. The sample cross-spectrum between $x_s(t_i)$ and $x_h(t_i)$ can be estimated by the cross periodogram, $I_{sh}(f)$ (f is the Fourier frequency, $f = \omega/2\pi$): $I_{sh}(f_i) = \{C_s(f_i)C_h(f_i) + S_s(f_i)S_h(f_i)\} + i\{C_s(f_i)S_h(f_i) - S_s(f_i)C_h(f_i)\}$, where $f_i = i/(N\Delta t)$, $i = 1, 2, \dots, N/2$, and $C(f_i), S(f_i)$ are the finite cosine and sine Fourier transforms of the data sets, i.e. $C(f_i) = \sqrt{\Delta t/N} \sum_j x(t_j) \cos(2\pi f_i t_j)$ and $S(f_i) = \sqrt{\Delta t/N} \sum_j x(t_j) \sin(2\pi f_i t_j)$.

In practice, it is customary to divide the light curve into many segments, compute the

cross periodogram for each of them, average $Re\{I_{sh}(f_i)\}$ and $Im\{I_{sh}(f_i)\}$ (where Re and Im denote the real and imaginary parts) and/or rebin them by averaging say m consecutive frequency bins to obtain an estimate of the cross-spectrum. In this case, the sample estimates of the phase spectrum and coherence function are given by, $\hat{\phi}_{sh}(f_i) = \tan^{-1}(\langle Im\{I_{sh}(f_i)\} \rangle / \langle Re\{I_{sh}(f_i)\} \rangle)$ and $\hat{\gamma}_{sh}(f_i) = \langle |I_{sh}(f_i)|^2 \rangle / \langle I_s(f_i) \rangle \langle I_h(f_i) \rangle$, where $|I_{sh}(f_i)|^2 = Re\{I_{sh}(f_i)\}^2 + Im\{I_{sh}(f_i)\}^2$, $I_s(f_i)$ and $I_h(f_i)$ are the periodograms of the individual light curves, and the brackets denote an average over the ensemble of the sample cross spectra and periodograms and/or over m consecutive frequency bins.

2.3. The NGC 7469 light curves

We have used the data from the ~ 30 day long *RXTE* observation of NGC 7469 in June/July 1996 in order to calculate the phase spectrum and the coherence function between light curves at different energy bands. We extracted light curves in the energy bands 2 – 4, 4 – 10 and 10 – 15 keV from the top layer of the proportional counter array (PCA). Full details of the PCA data analysis are given in Nandra et al. (2000) and NP01. We have used bin sizes of 5760s (\sim the *RXTE* orbital period) and 16s for the analysis.

There are $N = 480$ points in the 5760 sec binned light curves. Firstly, we calculated the real and imaginary part of the cross-spectral function between the 2 – 4/4 – 10 keV and 2 – 4/10 – 15 keV light curves. We also calculated the sample power spectra of the individual light curves (see section 5.1 in NP01). The light curves are not long enough to divide them into smaller segments so we simply grouped the real and imaginary parts of the cross periodogram into bins of size m and accepted them as our final estimates of the cross-spectrum at the mean frequency of each bin. For the 2 – 4/4 – 10 keV cross spectrum, we chose a value of $m = 10$ for the two lowest frequency bins (in order to extend the sample cross-spectrum estimation to the lowest possible frequencies) and $m = 35$ for the remaining bins. For the 2 – 4/10 – 15 keV cross spectrum, we used a value of $m = 15$ for the two lowest frequency bins and $m = 60$ for the higher frequency bins. The larger m value is necessary in this case as the Poisson noise level is more prominent in the 10-15 keV band (see below).

In order to extend the phase spectrum and coherence function estimation at the highest possible frequency we used the 230 parts of the 16 sec binned light curves that have no gaps in them (see NP01) and estimated the sample cross periodogram as before. We then combined all of them, sorted them in order of increasing frequency and grouped them in bins of size 60 for both cross spectra.

Poisson noise in the X-ray light curves affects the estimation of both the phase spectrum

and coherence function (for a detailed discussion see Vaughan and Nowak 1997, Nowak et al. 1999a). For this reason, we corrected for the Poisson noise power level the sample auto and cross-power spectra used in the calculation of the coherence function as described by Vaughan and Nowak (1997). We used their equation (8) to measure the uncertainty in the estimates of the coherence function and equation (16) from Nowak et al. 1999a in order to estimate the uncertainty in the sample phase spectra.

3. RESULTS

Our results for the 2–4/4–10 and 2–4/10–15 keV light curves are shown in Fig. 1 and 2. Fig. 1 shows the “time lags” (i.e. the phase spectrum divided by $2\pi f$) as a function of the Fourier period (i.e. $1/f$). The time lags for the 2–4/4–10 keV light curves are all positive and increase with period. The positive value indicates that components at frequency f in the 4–10 keV band are delayed with respect to the same components in the 2–4 keV band. The amount of the delay does not remain constant but increases with period. A constant lag does not give a good fit to the data ($\chi^2 = 58.8/8$ d.o.f). For the components at period ~ 3 ksec the delay is ~ 100 sec, increasing to ~ 10 ksec for components at period ~ 500 ksec (~ 6 days). We observe very similar behavior for the time lags between the 2–4 and 10–15 keV light curves. The determination of the lags is less precise in this case, however, and in fact one of the points in the 2–4/10–15 keV time lags plot is negative. When calculated using the 16sec binned light curves, the errors in the phase spectra are large at all but the lowest frequency point, and only this is plotted in Fig. 1. We have fitted a power law model to the time lag plots, with a slope of ~ 1 fitting both datasets well.

Fig. 2 shows the coherence functions. Although the uncertainties are rather large at high frequencies, our results suggest that intrinsic coherence is roughly unity for both the 2–4/4–10 and 2–4/10–15 keV bands over \sim two decades of frequencies.

3.1. Simulations

We have performed light curve simulations to validate the significance of the time lag detection. Our first set of simulations investigates the effects of Poisson noise which contributes a random component to the measured phase lag at each frequency. While this introduces an uncertainty, we do not expect that it will result in systematic lags between two time series, as we observe. We used the observed 2–4 keV, 5760s light curve as a template, and created 1000 pairs of light curves by adding random noise to each point equal to the

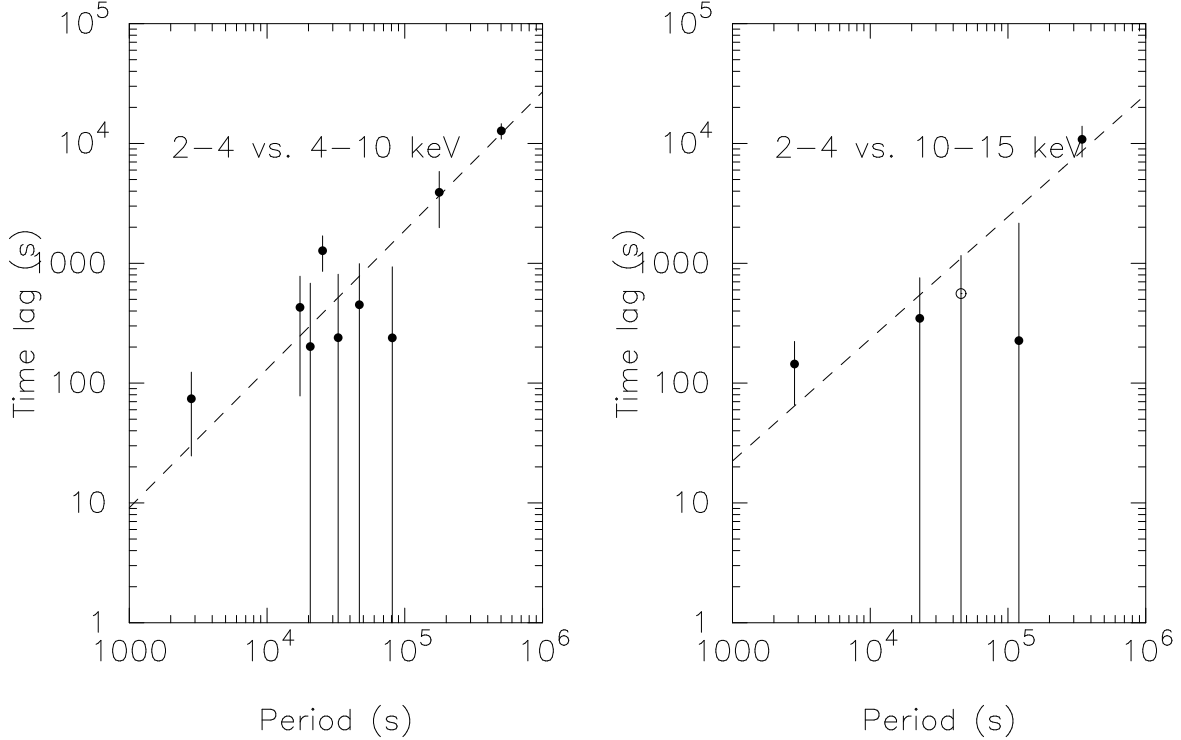


Fig. 1.— Time lag versus Fourier period ($1/f$) for the cross spectrum of the soft (2-4 keV) versus medium (4-10 keV) band (left panel) and the soft versus hard (10-15 keV) band (right panel). The lags have been binned as described in the text. The dashed lines show the best-fit power law model, which gives a good fit. In the former case this shows a slope of 1.2 ± 0.2 (68 per cent confidence for one interesting parameter) and normalization of 2.6×10^{-3} . The latter is much less well determined due to the higher Poisson noise level in the 10-15 keV band. Indeed the point shown with the open circle has a negative lag. Excluding that from the fit we find a best fit of 1.0 with a 90 per cent lower limit of 0.6 and no upper bound.

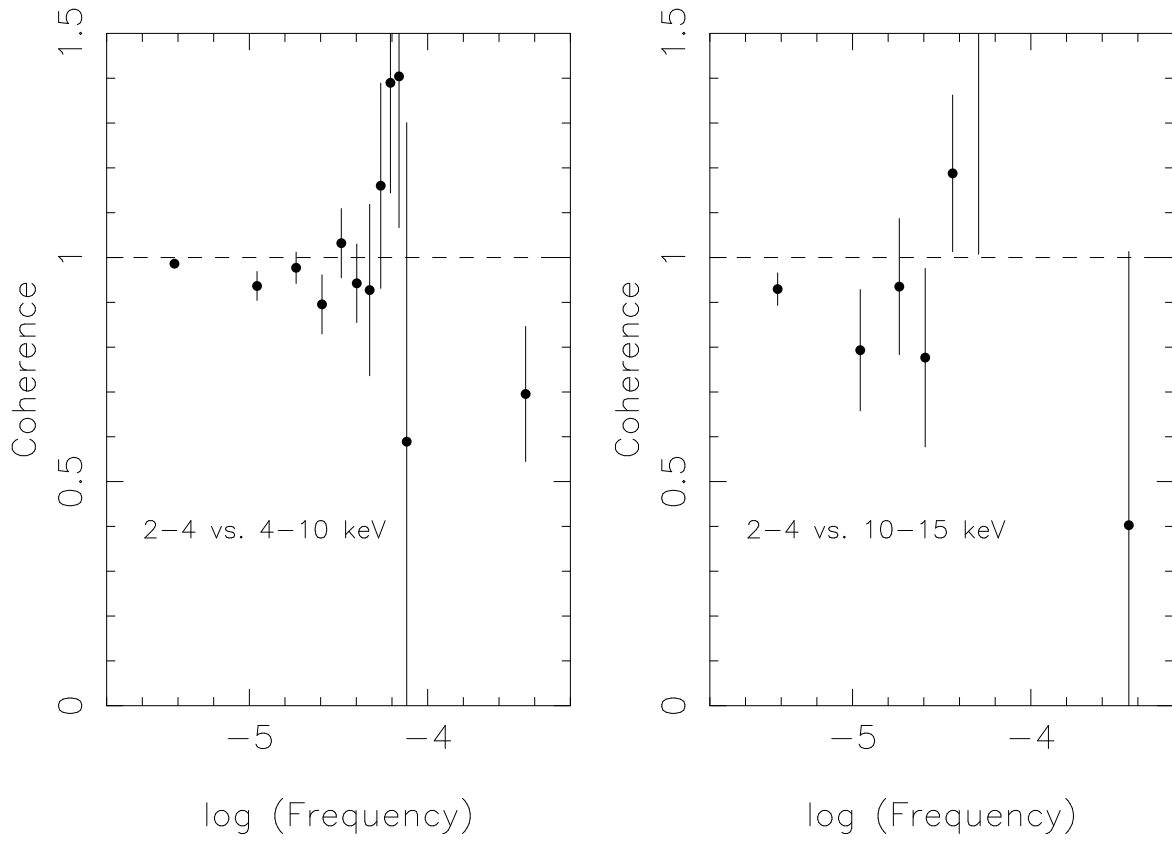


Fig. 2.— Coherence Fourier frequency soft versus medium band (left panel) and the soft versus hard band (right panel). The coherence is binned in the same way as the lags in Fig. ???. The values are close to or consistent with 1 (dashed line) similar to Cyg X-1.

average Poisson error of the observed light curves. The pairs were therefore identical (and hence have a coherence unity by construction), except for the effects of the Poisson noise and have no phase lags at any frequency. We computed the phase spectrum for each pair of light curves in the same way that we did for the actual data. The average lags were always very close to zero. Considering the two lowest frequency points in Fig 1a, the observed value was never achieved in the 1000 trials (also true of the point at period ~ 25 ksec). Furthermore, no phase spectrum of the 1000 synthetic light curves had all the estimated time lags being positive as we observe.

We then repeated this exercise using a randomly-generated light curve, rather than the real one, to investigate the effects of the red-noise character of the source variations. We assumed a PSD with a slope 1.5 appropriate for the 2-4 and 4-10 keV light curves (NP01), and created 1000 pairs. As before the pairs were identical except for differing Poisson noise. Our results were very similar as in the previous case. The two lowest frequency points in Fig. 1a have values larger than the time lags of all 1000 simulated light curves, and none of the 1000 phase spectra had all the points positive. We conclude that detection of lags in the phase spectrum shown in Fig. 1a cannot be the result of random, Poisson or red noise fluctuations in the 2 – 4/4 – 10 keV light curves.

Having established that the phase lags are not an artifact of Poisson or red noise in the data, we finally attempted to test whether the error prescription of Nowak et al. (1999a) is appropriate for our data. Although the dispersion of the points in the above simulations was found to be very similar to the calculated errors, a fairer test would be to simulate light curves with similar time lags to those observed in our data. We achieved this by performing a simulation similar to that just described, but shifted the phase of the sinusoids in the second series by the best-fit value obtained for the power law fit to the data in Fig. 1a. Random noise was then added to both series. Here we easily recovered the time lags from the simulated light curve: a positive lag was found for all 1000 simulations in the two lowest frequency bins. Furthermore, the dispersion on the simulated legs was very similar to the errors prescription of Nowak et al. (1999a), validating that technique for our data set.

4. DISCUSSION

We have presented the first cross-spectral analysis of the X-ray emission of a Seyfert galaxy, NGC 7469. We find time lags in the sense that the hard X-ray emission is delayed with respect to the soft. The estimated phase spectra have a rather large uncertainty, nevertheless the observed lags are consistent with being proportional to the variability time scale with a magnitude that is approximately 1 per cent of the Fourier period. The detection of frequency

dependent time lags is consistent with the results from the cross-correlation analysis of the X-ray light curves of NGC 7469 (NP01). The CCF shows no peak at time different than zero lag and it is asymmetric, in the sense that the soft X-rays lead the hard by a fraction of a day. The sense and magnitude of this asymmetry is consistent with the time lags we observe in the cross spectrum: although the peak of the CCF is dominated by the fastest variations, the asymmetry is caused by the relative delays between the two bands in the longer time scales. Finally, we find that the emission in the 2-4, 4-10 and 10-15 keV bands is highly coherent.

An obvious conclusion from Fig. 1 is that the lags in NGC 7469 resemble very closely those in the best studied galactic X-ray source, namely Cyg X-1 in its hard state (Miyamoto et al. 1992), but scaled by a factor $\sim 10^6$. Indeed, both the dependence of the lags on the Fourier period and their magnitude as a fraction of the given period ($\simeq 10^{-2}$) are very similar to those observed both in GBHC (Hua, Kazanas & Cui 1999) and neutron stars (Ford et al 1999).

The presence of lags in the sense we observe in our light curves offers strong additional support to the hypothesis that the X-ray are most likely due to Comptonization of soft photons by hot, thermal electrons. Such a hypothesis is consistent with both the X-ray spectra (Gondek et al. 1996) and the relationship between the seed photon flux and X-ray spectral shape (Nandra et al. 2000; Petrucci et al. 2000). In addition, the magnitude and period dependence of the lags places constraints on the processes responsible for the emission of radiation and the associated variability. There are several different models which account for these effects, and these can be divided into two broad classes:

(a) Models in which the lags result from the excess time the hard photons spend in the Comptonizing electron cloud before they escape (Kazanas, Hua & Titarchuk 1997; Hua, Kazanas & Titarchuk 1997). Because the propagation speed is that of light, the observed lags afford an estimate of the size the X-ray source. The longest observed lag in our dataset is $\sim 12,000s$ and Collier et al. (1998) estimated the mass of the black hole in NGC 7469 to be $8 \times 10^6 M_{\odot}$. These models therefore imply a size for the region of at least $240M_7^{-1} R_g$, where M_7 is the black hole mass in units of $10^7 M_{\odot}$ and R_g the gravitational radius. Our dataset does not sample periods longer than $\sim 10^6s$, but if the trend of lag increasing with period continues, the implied radius would be even larger. Having such an extended Comptonizing region raises the question of the plasma heating process. ADAF models (e.g. Narayan & Yi 1994) appear to provide a natural mechanism, but they also predict the dependence of the lags on the Fourier period to the radial density profile of the Comptonizing electrons. The linear dependence of the lag on the Fourier period we observe argues for an electron density profile $n(r) \propto r^{-1}$. This profile is not consistent with the ADAF solution, but it is consistent

with its variant ADIOS (Blandford & Begelman 1999). The models of this class, as presented to date, have employed an electron temperature which is independent of both radius and time. However, the electron temperature is expected to decrease within the ADAF models at a distance larger than $\sim 10^3 R_g$ while photon cooling should also contribute to the time dependence of the electron temperature. Indeed, the inclusion of time-dependent Compton cooling leads to significant modifications of the results compared to a static-corona case (Malzac & Jourdain 2000). Recently, Böttcher (2001) has shown that a model with a slab corona geometry (e.g. Haardt & Maraschi 1991) and a small-scale flare of the underlying, optically thick accretion disk, can explain well the overall shape of the time lag spectra in GBHC without a large corona when the effects of cooling due to the soft photon input is taken into account.

(b) Models in which the lags are produced by a spectral evolution of the X-ray emission (from soft to hard) due to coherent changes in the emission region (Poutanen & Fabian 1999; Böttcher & Liang 1999; Nowak et al. 1999b). The magnitude and sign of the lags in this class of models are obtained by a systematic hardening of the X-ray emission with time. The observed lags then, along with an estimate of the characteristic size of emission (a few tens of Schwarzschild radii), leads to a characteristic speed for effecting the change responsible for the observed X-ray variability. These speeds are generally much lower than those generally associated with dynamical and thermal time scales in the corresponding radii.

In conclusion, the time lags in the X-ray light curve of NGC 7469 are very similar to those observed in the X-ray light curves of GBHC. This - along with the corresponding PSDs - provides further evidence that the processes which determine the dynamics of accretion and the emission of X-ray radiation scale roughly linearly with the mass of the accreting object.

We thank the *RXTE* team for their operation of the satellite. IEP thanks the LHEA for their hospitality, and USRA for financial support. KN is supported by NASA grant NAG5-7067 provided through the Universities Space Research Association.

REFERENCES

- Blandford, R.D., Begelman, M.C., 1999, MNRAS, 303, L1
- Böttcher, M. 2001, ApJ, in press (astro-ph/0012269)
- Böttcher, M., Liang, E.P., 1999, ApJ, 511, L37
- Collier, S., et al., 1998, ApJ, 500, 162
- Edelson, R.A., Nandra, K., 1999, ApJ, 514, 682
- Ford E.C., van der Klis, M., Mendez, M., van Paradijs, J., Kaaret, P., 1999, ApJ, 512, L31
- Gondek, D., Zdziarski, A.A., Johnson, W.N., George, I.M., McNaron-Brown, K., Magdziarz, P., Smith, D., Gruber, D.E., 1996, MNRAS, 282, 646
- Haardt, F., Maraschi, L., 1991, ApJ, 380, L51
- Hua, X.-M., Kazanas, D., Titarchuk, L., 1997, ApJ, 482, L57
- Hua, X.-M., Kazanas, D., Cui, W., 1999, ApJ, 512, 793
- Kazanas, D., Hua, X.-M., Titarchuk, L., 1997, ApJ, 480, 735
- Malzac, J., Jourdain, E., 2000, A&A, 359, 843
- McHardy, I.M., Papadakis, I., Uttley, P., 1998, in *The Active X-ray Sky: results from BeppoSAX and RXTE*, L. Scarsi, H. Bradt, P. Giommi, and F. Fiore, Eds. (Amsterdam: Elsevier), p. 509
- Miyamoto, S., Kitamoto, S., Mitsuda, K., Dotani, T., 1988, Nature, 336, 450
- Miyamoto S., Kimura K., Kitamoto S., 1991, ApJ, 383, 784
- Miyamoto, S., Kitamoto, S., Iga, S., Negoro, H., Terada, K., 1992, ApJ, 391, 21L
- Narayan, R., Yi, I., 1994, ApJ, 428, L13
- Nandra, K., et al., 2000, ApJ, 544, 734
- Nandra, K., et al., 1998, ApJ, 505, 594
- Nandra, K., Papadakis, I.E., 2001, ApJ, in press (NP01)
- Nowak, M., Chiang, J., 2000, ApJ, 531, L13
- Nowak, M.A., Vaughan, B.A., Wilms, J., Dove, J. B., Begelman, M. C., 1999a, ApJ, 510, 874
- Nowak, M.A., Wilms, J., Vaughan, B.A., Dove, J. B., Begelman, M. C., 1999B, ApJ, 515, 726
- Petrucci, P.-O. et al., 2000, ApJ, 540, 131

- Pietrini, P., Krolik, J.H., 1995, ApJ, 447, 526
Poutanen, J., Fabian, A.C., 1999, MNRAS, 306, L31
Shapiro, S.L., Lightman, A.P., Eardley, D.M., 1976, ApJ, 204, 187
Sunyaev, R.A., Titarchuk, L.G., 1980, A&A, 86, 121
Vaughan B.A., Nowak, M.A., 1997, ApJ, 474, L43